Hyperfine structure in the sequence of sodium S states

Lundberg, Hans; Martensson, A-M; Svanberg, Sune

Published in:
Journal of Physics B: Atomic and Molecular Physics

DOI:
10.1088/0022-3700/10/10/026

1977

Hyperfine structure in the sequence of sodium S states

1977 J. Phys. B: At. Mol. Phys. 10 1971

(http://iopscience.iop.org/0022-3700/10/10/026)

J. Phys. B: Atom. Molec. Phys., Vol. 10, No. 10, 1977. Printed in Great Britain.

Hyperfine structure in the sequence of sodium S states

H Lundberg, A-M Mårtensson and S Svanberg
Department of Physics, Chalmers University of Technology, S-402 20 Göteborg, Sweden

Received 5 January 1977

Abstract. The hyperfine structure for the 6, 7 and 8 $^2S_{1/2}$ states of ^{23}Na was measured by optical double-resonance techniques. The states were populated by step-wise excitation using two CW dye lasers. For the dipole interaction constant a we obtain: $a(6^2S_{1/2}) = 37{\cdot}5(2)$ MHz, $a(7^2S_{1/2}) = 20{\cdot}9(1)$ MHz, $a(8^2S_{1/2}) = 12{\cdot}85(10)$ MHz. Theoretical calculations of the hyperfine structure were performed for the 3–8 $^2S_{1/2}$ states using many-body perturbation techniques. When polarization as well as certain correlation effects are included in the calculation, an agreement with the experimental values within 2% is obtained.

1. Introduction

During recent years the methods for the calculation of atomic structure have been greatly improved, e.g. by the application of many-body theory to atomic problems. At this laboratory techniques for the calculation of fine structure (Holmgren *et al* 1976), as well as hyperfine structure (Garpman *et al* 1975, 1976, Lindgren *et al* 1976), for alkali atoms have been developed. With the introduction of new experimental techniques the possibilities for accurate determinations of small energy intervals have been greatly extended, and the knowledge of the fine and hyperfine structure in alkali atoms has recently been considerably increased. The light alkali atoms are particularly suitable for a comparison between theory and experiment because of their simple electronic structure. In this work we report on the measurement of the hyperfine structure (HFS) for the 6, 7 and $8^2S_{1/2}$ sodium states and on theoretical hyperfine calculations for the sequence of sodium S states, using many-body perturbation techniques.

In the development of several new laser spectroscopic techniques, sodium has attracted a great deal of interest. For example, the anomalous fine-structure in the sequence of D states has been extensively investigated in two-photon absorption, quantum-beat, and level-crossing experiments (Salour 1976, Fabre *et al* 1975, Fredriksson and Svanberg 1976). On the other hand, comparatively few hyperfine structures have been accurately measured. For the S sequence the ground $3^2S_{1/2}$ state was studied a long time ago using the atomic-beam magnetic resonance and optical-pumping methods (Fuller and Cohen 1969). The $4^2S_{1/2}$ state was measured with RF spectroscopy by Liao *et al* (1973) employing cascade excitation from a higher P state. Using step-wise excitation involving a tunable laser, it is also possible to investigate highly excited S states, as first shown by Tsekeris *et al* (1974). With such techniques, the $5^2S_{1/2}$ state was measured by Tsekeris *et al* (1976). We have now

extended these measurements to the 6, 7 and $8^2S_{1/2}$ states, for which no accurate values were available. Only relatively crude values for the 6 and $7^2S_{1/2}$ state HFS were obtained in recent two-photon absorption experiments (Levenson and Salour 1974, Hawkins *et al* 1977).

2. Experimental arrangement

A schematic diagram of the experimental set-up is shown in figure 1. A quartz resonance cell was mounted in an RF coil inside an oven and heated to 115–125°C by a stream of hot air. The cell had been baked out at 400°C for two days with continuous high-vacuum pumping, before sodium was distilled into the cell and it was sealed off. The atoms were excited in two steps into the high S states, with the $3^2P_{3/2}$ state as an intermediate level, by the light from two tunable CW dye lasers.

A Coherent Radiation Model 490 dye laser, operating with rhodamine 6G and pumped by the visible lines of a CR8 argon-ion laser (~ 6 W), was used in the first step. For the second step we used a coumarine 47 or a coumarine 6 dye laser, pumped by a CR12 argon-ion laser, operating on the UV lines ($\sim 1{\cdot}5$ W) or on the 4880 Å line (~ 7 W), respectively. The multimode output power was about 500 mW for the rhodamine laser and about 100 mW for the coumarine laser. The laser beams were circularly polarized and were made to overlap within the cell, utilizing a blue-transmitting and yellow-reflecting dielectric mirror as shown in the figure. States with $J = \frac{1}{2}$ must be excited with circularly polarized light (σ^+ or σ^- excitation) in order to produce a non-uniform population of the magnetic sublevels. A small mirror on the magnetic field axis was used to reflect the laser light in the direction of the field through the cell. The fluorescent light was collected in a solid angle symmetric around this mirror. An EMI 9558 BQ photomultiplier tube detected at 330 nm fluorescent light released in the decay of the 4^2P levels which were populated in the cascade decay. The intense scattered light from the cell windows was efficiently suppressed with interference and Schott coloured-glass filters. Using a $\lambda/4$-plate and

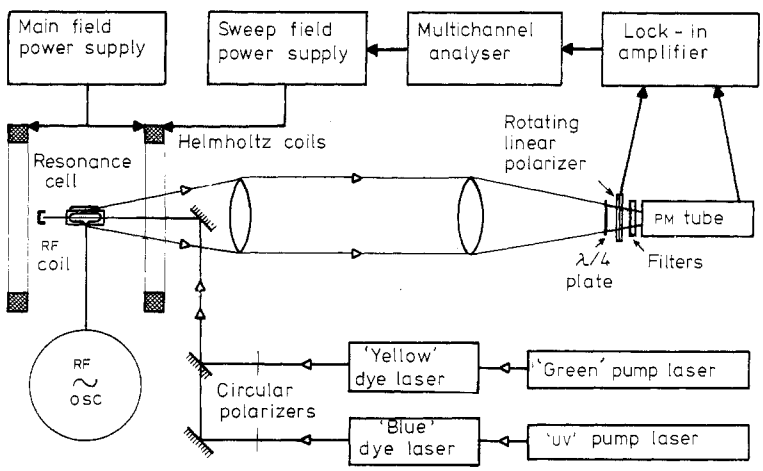

Figure 1. Schematic diagram of the experimental arrangement used in the optical double-resonance experiments.

a rotating Polacoat PL 40 linear polarizer in the detection light beam, the degree of circular polarization of the fluorescent light was measured, using lock-in technique. The reference signal for the lock-in amplifier was obtained from the rotating polarizer by means of a vane switch oscillator. The lock-in output signal was fed to a Laben Correlatron averaging multichannel analyser. A homogeneous magnetic field was applied over the resonance volume by two pairs of Helmholtz coils, one for a steady field and the other for a sweep field which was controlled by the multichannel analyser. The coil systems were calibrated by optical pumping in the ground state of caesium. Using a two-turn coil around the cell, an RF field perpendicular to the magnetic field was generated for inducing RF transitions.

3. Measurements

At the low sodium vapour pressure used in this experiment, no strong multiple scattering occurs in the first excitation step, which corresponds to one of the D lines ($3^2S_{1/2}$–$3^2P_{3/2}$). Thus, an orientation can, in contrast to the case in earlier experiments (e.g. Svanberg and Tsekeris 1975), be induced in the P state. By a subsequent excitation to the highly excited $^2S_{1/2}$ state, using circularly polarized laser light of opposite helicity, an enhanced orientation can be created in this state. In the branch decay of the $^2S_{1/2}$ state into the 4^2P states, the orientation is partly transferred. The fluorescent light at 330 nm, obtained in the decay of the P states, will then reflect this orientation in its polarization properties. The difference in intensity between right- and left-hand circularly polarized (σ^+ and σ^-) light, as measured with the lock-in detector, will be closely related to the original orientation of the highly excited $^2S_{1/2}$ state. By partly equalizing the populations of magnetic sublevels of this state, using a resonant RF field, the polarization of the 330 nm light will be decreased.

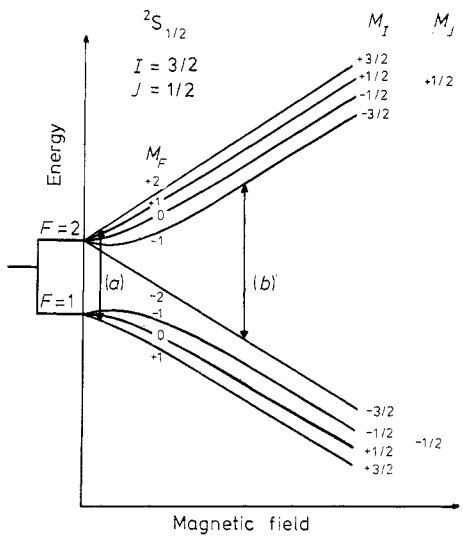

Figure 2. Breit–Rabi diagram for a $^2S_{1/2}$ state in ^{23}Na. The sublevels are characterized by the quantum number M_F in low fields and by the quantum numbers M_I and M_J in high fields. Two RF transitions, corresponding to the curves in figures 3 and 4, are indicated.

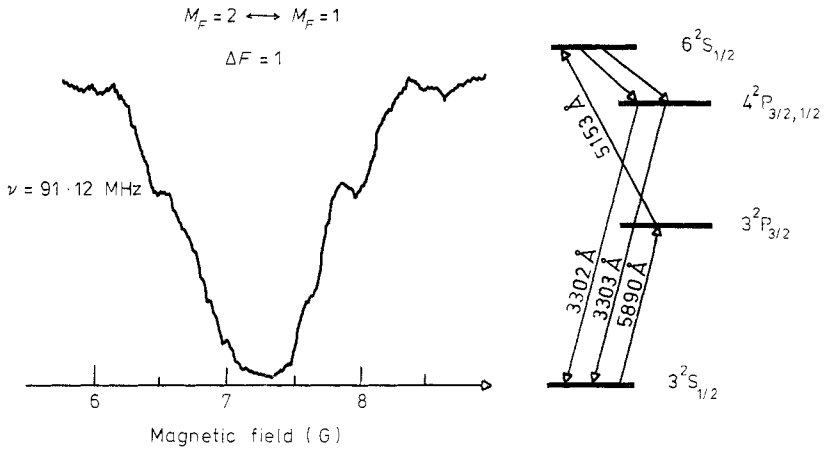

Figure 3. Excitation and detection scheme and a resonance curve for the $6^2S_{1/2}$ state. The integration time for this curve was about four hours.

For a $^2S_{1/2}$ state, the sublevel structure can be calculated as a function of an external magnetic field using the Breit–Rabi formula (Kopfermann 1958). In figure 2 the corresponding level scheme is shown. Due to the magnetic hyperfine interaction, the electronic level splits up into two HFS levels, with a separation of $2a$. Here a is the magnetic dipole interaction constant, which is the quantity of interest in this work. It can be measured by inducing RF transitions in zero magnetic field or in the presence of an external field. We chose to observe resonances either at low magnetic fields (close to the Zeeman region) or at high fields (close to the Paschen–Back region) as illustrated in the figure. For a fixed RF frequency, the magnetic field was repetitively swept through the region of resonance and the signals were accumulated in the multichannel analyser for reading out when a sufficient signal-to-noise ratio had been obtained. In order to eliminate influences of the earth's magnetic field and time constants in the electronics, data for each resonance were taken for the two directions of the steady magnetic field.

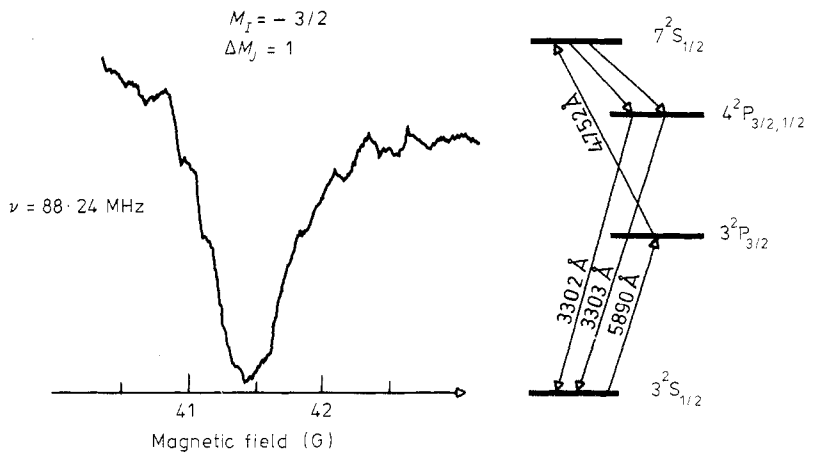

Figure 4. Excitation and detection scheme, and a resonance curve for the $7^2S_{1/2}$ state. The asymmetry of this curve is due to the presence of broad resonances in the $4^2P_{3/2}$ state at higher magnetic fields.

In figure 3 the excitation and detection scheme for the $6^2S_{1/2}$ state is shown together with a low field recording of the $\Delta F = 1$, $M_F = 2 \leftrightarrow M_F = 1$ resonance. The relative position of this transition is shown at (*a*) in figure 2. The measurements for the $7^2S_{1/2}$ state are illustrated in figure 4, where a high-field resonance, $\Delta M_J = 1$, $M_I = -\frac{3}{2}$, corresponding to (*b*) in figure 2, is shown. Similar measurements were made for the $8^2S_{1/2}$ state. For all the studied states, several resonances at different frequencies were recorded. The data were for each state fitted to the Breit–Rabi formula using a computer program. For the dipole interaction constants we obtain: $a(6^2S_{1/2}) = 37{\cdot}5(2)$ MHz, $a(7^2S_{1/2}) = 20{\cdot}9(1)$ MHz and $a(8^2S_{1/2}) = 12{\cdot}85(10)$ MHz. The error bars comprise two standard deviations of the statistical data as well as allowances for possible systematic errors.

4. Theoretical calculations

The hyperfine structure of sodium S states, which is very suitable for *ab initio* calculations, has previously been studied theoretically by e.g. Lee *et al* (1970) and Mahanti *et al* (1974). We have applied the technique, developed at this laboratory, for many-body calculations to determine the HFS in the sodium S sequence. The calculations are based on a perturbation expansion of effective operators, and a diagrammatic technique is employed (Garpman *et al* 1975).

The starting point for our calculation is the restricted Hartree–Fock (HF) model for the Na^+ ion. The HF value of the hyperfine interaction constant is represented by the diagram in figure 5(*a*). When we want to go beyond this model, the most important perturbations are the so-called core-polarization effects that can be regarded as distortions of the closed shells due to the interaction with the anisotropic open shell. The lowest-order contribution from this effect arises from the diagram in figure 5(*b*), which was also calculated for the sodium S states by Mahanti *et al* (1974). These effects can be included within an independent-particle model such

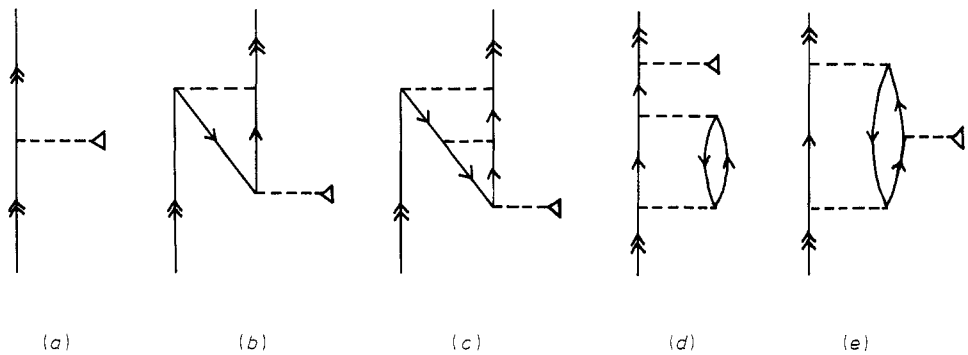

Figure 5. Diagrammatic representation of contributions to the magnetic dipole constant. Falling lines represent core orbitals, rising lines excited orbitals (single arrow) and open-shell orbitals (double arrows). A broken line represents an electrostatic interaction, a broken line with a triangle the hyperfine interaction. The following diagrams are shown (*a*) the zero-order (HF) contribution; (*b*) the lowest-order polarization contribution; (*c*) the next higher-order polarization contribution; (*d*) example of a 'self-energy' correlation diagram, and (*e*) example of a lowest-order correlation diagram which is not of the 'self-energy' type. (There are 24 such correlation diagrams, and they are all included in the calculation.)

Table 1. Results of the calculation of the magnetic dipole interaction constant (in MHz) for the 3, 5 and $7^2S_{1/2}$ states of ^{23}Na. (Relativistic effects are not included.)

		Orbitals used			
		HF	NO	Higher order NO	Experiment
$3^2S_{1/2}$	Zeroth order (figure 5(*a*))	616·7	707·8	717·2	
	+ Polarization	758·9	867·2	877·3	
	+ Correlation	794·0	849·4	860·7	885·82
$5^2S_{1/2}$	Zeroth order	57·4	62·9		
	+ Polarization	70·5	76·6		
	+ Correlation	73·1	75·3		77·6 (2)
$7^2S_{1/2}$	Zeroth order	15·7	17·0		
	+ Polarization	19·3	20·5		
	+ Correlation	19·5	20·4		20·9 (1)

as the unrestricted Hartree–Fock (UHF). Mathematically they are described as single excitations from the HF model and in our formalism are included by solving single-particle equations (Garpman *et al* 1975). If these equations are solved self-consistently, as described by Garpman *et al* (1976), these effects can be included to all orders, and we arrive at the UHF values. The first higher-order diagram is shown in figure 5(*c*). Effects beyond the UHF are referred to as correlation effects and they require multiple excitations in the mathematical description. The dominating part of the

Table 2. Experimental and theoretical dipole interaction constants for S states of ^{23}Na.

	Dipole interaction constant a(MHz)				
State	Experiment	HF	+ Polarization	+ Correlation	+ Relativistic effects
$3^2S_{1/2}$	885·82[a]	616·7	758·9 764·1[f]	860·7	872·5
$4^2S_{1/2}$	202 (3)[b]	148·9	182·8 184·1[f]		
$5^2S_{1/2}$	77·6 (2)[c]	57·4	70·5 71·9[f]	75·3	76·2
$6^2S_{1/2}$	37·5 (2) 39 (3)[d] 34·5 (4·5)[e]	28·0	34·3 33·7[f]		
$7^2S_{1/2}$	20·9 (1) 23·3 (6·5)[e]	15·7	19·3 19·8[f]	20·4	20·6
$8^2S_{1/2}$	12·85 (10)	9·8	12·0 12·2[f]		

[a]Fuller and Cohen (1969).
[b]Liao *et al* (1973).
[c]Tsekeris *et al* (1976).
All other results, this work.
[d]Levenson and Salour (1974).
[e]Hawkins *et al* (1977).
[f]Mahanti *et al* (1974).

correlation has been found to be of the 'self-energy' type, and is described by insertions of multiple excitations into single orbital lines in the diagrams (figure 5(*d*)). Other types of correlations are exemplified in figure 5(*e*). Lindgren *et al* (1976) show that the self-energy effect can be included in the orbitals, yielding approximate Brueckner or natural orbitals (NO). This means that diagrams of the type in figure 5(*d*) can be included in a diagram corresponding to figure 5(*a*). The effect on the orbitals is most significant for the valence orbital, which becomes more contracted due to the attraction of the 'correlation hole' created by the valence electron in the electron core. Using the natural orbitals, the diagrams corresponding to figures 5(*b*), (*c*) and (*e*) can be calculated, and will now implicitly include important additional correlation effects. The results of our calculations for the 3, 5 and $7^2S_{1/2}$ states are given in table 1. For the $3^2S_{1/2}$ state, results obtained using a new technique (Mårtensson 1977), by which essentially all pair-correlation effects can be included, are presented in the last column. Whereas the more complete calculations are restricted to the 3, 5 and $7^2S_{1/2}$ states, the polarization effect (using HF orbitals) is calculated for all S states studied so far. In table 2 the results are given. All the calculations are non-relativistic. The relativistic effect has been estimated using the correction factors calculated by Rosén and Lindgren (1972).

5. Discussion

In figure 6 we have plotted the ratio between the different theoretical values and the experimental value for the dipole interaction constant *a*. As can be seen, the Hartree–Fock theory describes the hyperfine structure of the studied S states rather poorly; it only accounts for about 75% of the experimental value. By adding polarization effects to all orders, the deviation from the measured values is decreased to about 10%. In the diagram the first-order polarization values, calculated by Mahanti *et al* (1974), are also indicated. These authors find that the polarization contribution

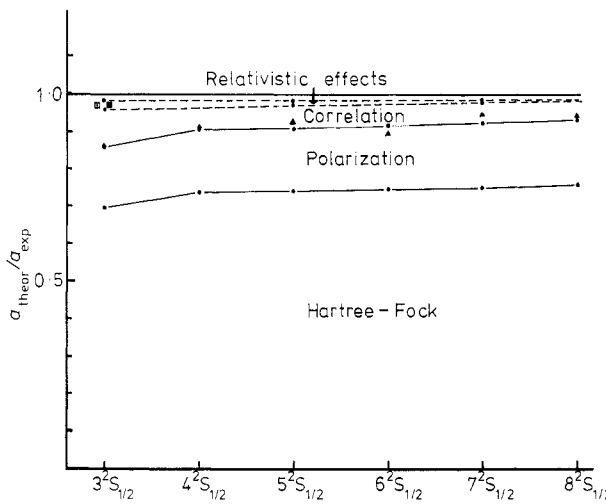

Figure 6. The ratio a_{theor}/a_{exp} plotted for the sequence of sodium S states. ●, this work; ▲, polarization values (Mahanti *et al* 1974); ⊡, final non-relativistic value for $3^2S_{1/2}$ (this work); ■, final non-relativistic value for $3^2S_{1/2}$ (Lee *et al* 1970).

is an almost constant fraction of the HF value for all the states. This is also true for our all-order polarization, and in our calculation the fraction is found to be 22·9 ± 0·2%. The agreement between the first-order polarization values, obtained by Mahanti *et al*, and our all-order calculation may seem surprisingly good at first sight. However, the V^{N-1} potential used by Mahanti *et al* yields essentially the diagonal parts of the higher order polarization when the first order is evaluated (random-phase approximation) (Chang and Fano 1976, I Lindgren 1976 private communication). We have found that the off-diagonal parts are insignificant for the sodium S states.

In the calculation of Mahanti *et al* an anomalously low value is obtained for the $6^2S_{1/2}$ state, due to a low HF value for that state.

Our values for the 3, 5 and $7^2S_{1/2}$ states, calculated using approximate natural orbitals also including correlation effects (column 2 of table 1) are plotted in the diagram. For the higher states the values are now within 3% from experiment. The agreement is slightly worse for the $3^2S_{1/2}$ state. However, by adding the next higher order correlation effect, which seems to be more important for the lowest state than for the higher ones, this value (indicated by ⊡) comes closer to experiment. For this state the value of Lee *et al* (1970) (a = 857·8 MHz), which includes the lowest order correlation, is also shown (indicated by ■).

By also including relativistic effects, which can be done by applying correction factors (Rosén and Lindgren 1972), our final values deviate from the experimental results by only 1·5%. The remaining discrepancy might be explained by numerical uncertainties, higher order correlation and genuine three-body effects.

Acknowledgments

The authors are very grateful to Professor Ingvar Lindgren for most valuable advice, particularly concerning the theoretical calculations. This work was financially supported by the Swedish Natural Science Research Council.

References

Chang T N and Fano U 1976 *Phys. Rev.* A **13** 263–81
Fabre C, Gross M and Haroche S 1975 *Opt. Commun.* **13** 393–7
Fredriksson K and Svanberg S 1976 *J. Phys. B: Atom. Molec. Phys.* **9** 1237–46
Fuller G H and Cohen V W 1969 *Nuclear Data Tables* ed K Way (New York: Academic Press)
Garpman S, Lindgren I, Lindgren J and Morrison J 1975 *Phys. Rev.* A **11** 758–81
——1976 *Z. Phys.* A **276** 167–77
Holmgren L, Lindgren I, Morrison J and Mårtensson A-M 1976 *Z. Phys.* A **276** 179–85
Hawkins R T, Hill W T, Kowalski F V, Schawlow A L and Svanberg S 1977 *Phys. Rev.* A **15** 967–74
Kopfermann H 1958 *Nuclear Moments* (New York: Academic Press)
Lee T, Dutta N C and Das T P 1970 *Phys. Rev.* A **1** 995–1006
Levenson M D and Salour M M 1974 *Phys. Lett.* **48A** 331–2
Liao K H, Gupta R and Happer W 1973 *Phys. Rev.* A **8** 2811–3
Lindgren I, Lindgren J and Mårtensson A-M 1976 *Z. Phys.* A **279** 113–25
Mahanti S D, Lee T and Das T P 1974 *Phys. Rev.* A **10** 1091–5
Rosén A and Lindgren I 1972 *Phys. Scr.* **6** 109–21
Salour M M 1976 *Opt. Commun.* **18** 377–80
Svanberg S and Tsekeris P 1975 *Phys. Rev.* A **11** 1125–37
Tsekeris P, Gupta R, Happer W, Belin G and Svanberg S 1974 *Phys. Lett.* **48A** 101–2
Tsekeris P, Liao K H and Gupta R 1976 *Phys. Rev.* A **13** 2309–10